

DIRECT MEASUREMENT OF THE RATIO OF CARBON MONOXIDE TO MOLECULAR HYDROGEN IN THE DIFFUSE INTERSTELLAR MEDIUM

ERIC B. BURGH

Space Astronomy Laboratory, University of Wisconsin, Madison, WI; ebb@sal.wisc.edu

AND

KEVIN FRANCE¹ AND STEPHAN R. McCANDLISS

Department of Physics and Astronomy, The Johns Hopkins University, Baltimore, MD

Received 2006 July 26; accepted 2006 November 21

ABSTRACT

We have used archival far-ultraviolet spectra from observations made by *HST* STIS and *FUSE* to determine the column densities and rotational excitation temperatures for carbon monoxide and molecular hydrogen, respectively, along 23 sight lines to Galactic O and B stars. The reddening values range from $E(B - V) = 0.07$ to 0.62, sampling the diffuse to translucent interstellar medium (ISM). We find that the H_2 column densities range from 5×10^{18} to $8 \times 10^{20} \text{ cm}^{-2}$ and the CO from upper limits around $2 \times 10^{12} \text{ cm}^{-2}$ to detections as high as $1.4 \times 10^{16} \text{ cm}^{-2}$. CO increases with increasing H_2 , roughly following a power law of factor ~ 2 . The CO/ H_2 column density ratio is thus not constant, ranging from 10^{-7} to 10^{-5} , with a mean value of 3×10^{-6} . The sample segregates into “diffuse” and “translucent” regimes, the former with molecular fraction $\lesssim 0.25$ and $A_V/d < 1 \text{ mag kpc}^{-1}$. The mean CO/ H_2 for these two regimes are 3.6×10^{-7} and 9.3×10^{-6} , respectively, significantly lower than the canonical dark cloud value of 10^{-4} . Six sight lines show the isotopic variant ^{13}CO , and the isotopic ratio we observe (~ 50 – 70) is consistent with, if perhaps a little below, the average $^{12}\text{C}/^{13}\text{C}$ for the ISM at large. The average H_2 rotational excitation temperature is $74 \pm 24 \text{ K}$, agreeing well with previous studies, and the average CO temperature is 4.1 K, with some sight lines showing temperatures as high as 6.4 K. The higher excitation CO is observed with higher column densities, consistent with the effects of photon trapping in clouds with densities in the 20 – 100 cm^{-3} range. We discuss the implications for the structure of the diffuse/translucent regimes of the ISM and the estimation of molecular mass in galaxies.

Subject headings: ISM: abundances — ISM: clouds — ISM: lines and bands — ISM: molecules — ISM: structure

Online material: color figures

1. INTRODUCTION

Molecular hydrogen (H_2) is the most abundant molecule in the interstellar medium (ISM), residing primarily in the large complexes of the dense molecular clouds that account for 10%–20% of the mass in the inner disk of the Galaxy (Shull & Beckwith 1982). However, it is difficult to observe directly. H_2 is a homonuclear molecule, with quadrupolar ground-state transitions that emit radiation only very weakly. Carbon monoxide (CO), in contrast, has strong ground-state transitions that produce readily observable emissions at radio wavelengths. In clouds with densities above the critical density for CO, H_2 collisions dominate the ground-state excitation, and thus CO radio emission acts as a tracer of H_2 in these regions.

This relationship is often characterized by the conversion factor $X = N(H_2)/I_{\text{CO}}$, where I_{CO} is the integrated brightness temperature of the $J = 1$ – 0 radio emission line at 2.6 mm. The value for the conversion factor is generally determined by one of the following techniques (Young & Scoville 1991): correlation of the CO emission with A_V in clouds determined by star counts, which is then correlated with H_2 by the extrapolation of the N_H/A_V from the diffuse ISM (Savage et al. 1977); an excitation analysis of ^{13}CO , assuming it is optically thin, ^{12}CO is optically thick, and the $^{12}\text{CO}/^{13}\text{CO}$ is known; a virial analysis using the cloud sizes

and line widths; and comparison with γ -ray emission (e.g., Strong & Mattox 1996). These techniques produce a value for X of about $2 \times 10^{20} \text{ cm}^{-2} (\text{K km s}^{-1})^{-1}$, but examples of up to a factor of 10 higher can be found in the literature.

It is generally recognized that CO emission can qualitatively trace the distribution of H_2 in the ISM, but because of difficulties in translating a measurement of $I_{\text{CO}}(1-0)$ into a column density of CO, X is not a good quantitative measure of $N(\text{CO})/N(H_2)$ (hereafter CO/ H_2). To relate X to a relative column density ratio requires the assumption of local thermodynamic equilibrium (LTE) and is typically done with the unsaturated ^{13}CO radio lines, so one must also assume excitation temperatures and abundance ratios for the two CO isotopes. This exercise gives a value of CO/ H_2 of about 10^{-4} for the dense molecular clouds, but with a large uncertainty (e.g., Dickman 1978).

The determination of CO/ H_2 is simplified by the direct observation of the two species in absorption. This has been done in the infrared, using vibrational transitions, and values of $\sim (2-3) \times 10^{-4}$ were found for the molecular clouds in NGC 2024 and NGC 2264 (Lacy et al. 1994). With ultraviolet observations, this direct method can be extended to the diffuse and translucent phases of the ISM, where the molecules are more susceptible to the effects of photodissociation, and thus, CO/ H_2 is expected to vary relative to the dense clouds. Models suggest that the photodissociation of CO is sensitive, even more so than H_2 , to the strength of the interstellar ultraviolet radiation field, cloud geometry, and the ultraviolet absorption and scattering properties of dust (van Dishoeck & Black

¹ Current address: Canadian Institute for Theoretical Astrophysics, University of Toronto, Toronto, ON.

1988; Kopp et al. 2000). Therefore, the interrelationship between CO and H₂ may also be a good measure of the physical conditions and structure of the diffuse and translucent regimes of the ISM. Furthermore, there is evidence that a significant contribution to the large-scale Galactic CO emission is made by lower optical depth gas (Polk et al. 1988).

H₂ is best observed in the far-ultraviolet, where there are extensive dipole-allowed electronic absorption band systems. The *Far Ultraviolet Spectroscopic Explorer* (*FUSE*) has proven to be an excellent instrument for studying H₂ in absorption (see, e.g., Rachford et al. 2002; Tumlinson et al. 2002; Gillmon et al. 2006). CO also has an absorption band system throughout the ultraviolet, and a study of CO in the diffuse ISM using *Copernicus* was performed by Federman et al. (1980) and later reanalyzed by Crenny & Federman (2004). These observations were limited to the *C–X* (1088 Å) and *E–X* (1076 Å) absorption bands toward 48 nearby bright stars, with only about one-third having CO, some of those being saturated. Furthermore, the spectral resolution ($R \sim 20,000$) was not high enough to resolve the rotational substructure of the bands. Federman et al. (1980) concluded that measurements with a more sensitive, higher spectral-resolution instrument would allow for a better understanding of the relationship between H₂ and CO across a wider range of environments.

This can be achieved using the Space Telescope Imaging Spectrograph (STIS) on board the *Hubble Space Telescope*, which has access to the fourth positive ($A^1\Pi-X^1\Sigma^+ v''=0$) band system. More than a dozen absorption bands from the ground vibrational state of CO have been detected, and because of the large variance in oscillator strengths, they probe a variety of optical depths, allowing for an accurate determination of column density. In addition, with the highest resolution grating modes (E140H) these bands can be resolved clearly into their constituent rotational structure. Because the rotational levels in the ground state of CO are closely spaced, the rotational excitation temperature of the molecule is easily determined.

Pan et al. (2005) used STIS Echelle and *FUSE* data to explore the CO and H₂ absorptions in the Cepheus OB2 and OB3 clusters. They find evidence for systematic variations in CO/H₂ in these two different star-forming regions, which they say may indicate differences in star-formation histories. In this paper, we broaden the study of CO/H₂ to the diffuse molecular regime of the ISM, rather than study isolated regions. We present an analysis of 23 stars, which have been observed by both *FUSE* and the STIS E140H mode. The reddening of these stars range from $E(B - V) = 0.07$ to 0.62, complementing the Pan et al. study well, whose sight lines range from $E(B - V) = 0.35$ to 0.86. The H₂ and CO absorptions have been measured and column densities and rotational temperatures determined. These data provide a survey of the CO/H₂ relationship in the diffuse to translucent molecular regime of the ISM.

2. DATA AND ANALYSIS

The data presented here were retrieved from the Multimission Archive at STScI (MAST). The STIS observations employed the E140H grating, providing the highest possible spectral resolution. The wavelength coverage of STIS allows for the observation of a number of absorption bands of the CO *A–X*($v''=0$) band system. For some of the stars, however, the specific tilt of the Echelle grating allows for observation of only higher vibrational bands ($v'' \geq 7$), because of the more blueward wavelength coverage. The *FUSE* data were processed with the CalFUSE pipeline, version 2.2. The individual channels (e.g., LiF 1a and SiC 1a) were joined using an IDL shifting routine written to combine

time-tagged or histogrammed *FUSE* data. In addition, we obtained STIS data corresponding to five sight lines from a *FUSE* survey of translucent clouds (Rachford et al. 2002), from whom we obtained the H₂ column densities.

2.1. Carbon Monoxide

CO has an extensive electronic absorption band system, the fourth positive ($A^1\Pi-X^1\Sigma^+$) system, ranging from 1510 Å to shorter wavelengths. Because the energies of the rotational levels in the ground state of CO are closely spaced, the relative strengths of the individual rovibrational transitions are very sensitive to excitation temperature. Previous surveys, such as Federman et al. (1980), used *Copernicus* data, which were not able to resolve the rotational structure; however, the high spectral resolution of the STIS E140H grating ($R = \lambda/\Delta\lambda = 110,000$) allows these transitions to be well resolved from each other and provides for an accurate determination of the rotational temperature in addition to column density.

Model spectra of the rovibrational absorption were generated using the wavelengths and oscillator strengths of Morton & Noreau (1994). The best-fit model was chosen using a χ^2 statistic from a grid corresponding to varying column density (N), rotational excitation temperature (T_{rot}), and Doppler line-broadening parameter, b . For most of the low-column sight lines, the bands (1–0) through (5–0) were fit simultaneously. For sight lines with only the shorter wavelength data, the bands starting with (7–0) and higher were fit. Figure 1 shows a sample of spectra with five bands of the *A–X* system range in column densities with corresponding best-fit models overlaid. When the lower vibrational bands were available, the detection limit was typically $N \sim 2.5 \times 10^{12} \text{ cm}^{-2}$. For the (7–0) band, it was $N \sim 4.0 \times 10^{13} \text{ cm}^{-2}$. In all but four of the sight lines, CO absorption was detected, and in six of the higher column sight lines the isotopic variant ¹³CO was also observed.

In addition to the profile fitting, a curve-of-growth (COG) analysis was performed for each sight line. The individual rovibrational absorption profiles of each available band were fitted with Gaussians, their equivalent widths measured, and a COG constructed. A similar grid-search process as used in the profile fitting was employed and the N , T_{rot} , and b determined by comparison to the theoretical COG for a single velocity component. For sight lines with column densities below 10^{14} cm^{-2} , the best-fit values agree with those determined from the profile-fitting process within the error.

For the higher column sight lines, unresolved velocity components may influence the results. The equivalent width of an absorption line can be higher for a given total column density if the velocity structure contains unresolved nonoverlapping absorption lines. This effect is more pronounced as the lines become saturated, and thus the equivalent widths of the higher oscillator strength bands are inflated, producing a COG that mimics that of a single component with higher b . However, if enough unsaturated lines can be observed, then the column density determination is still robust. The combination of the STIS signal-to-noise ratio and high spectral resolution allow, in virtually all cases, for the observation of absorption lines that lie on the linear part of the COG. We noted that for values of b above $\sim 0.6 \text{ km s}^{-1}$, saturation effects are mild to negligible for absorption lines with an $Nf\lambda \leq 10^{15} \text{ cm}^{-2} \text{ \AA}$.

Our initial fits of the higher column sight lines produced b -values in the range 1.0–3.0. These are higher than expected for molecular material (Pan et al. [2004] find $b = 0.6$ –1.0 for CN, for example). We found that by limiting the fitting process to only the weaker absorptions, we were able to reproduce the lower b -values.

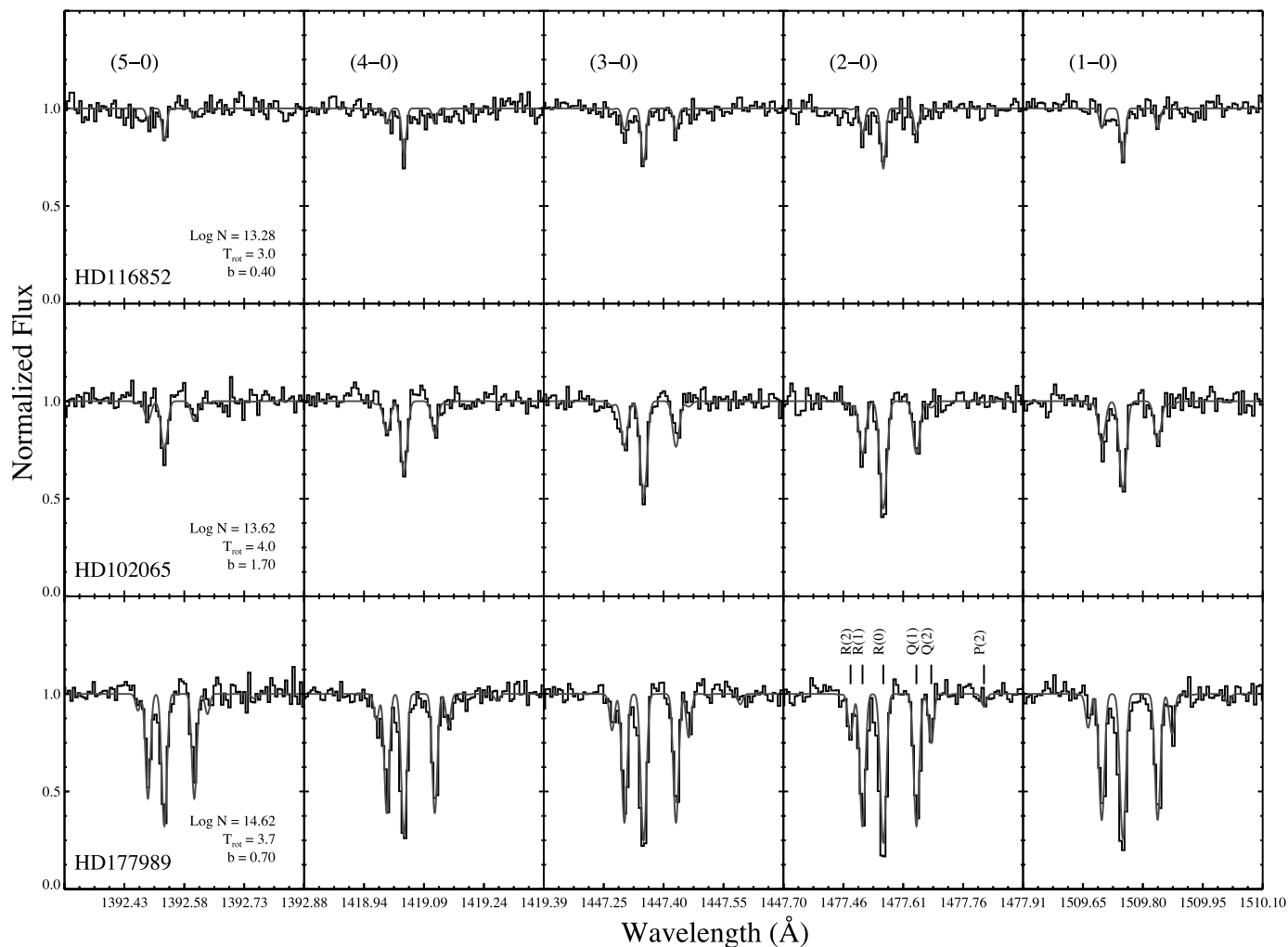


Fig. 1.— Sample CO absorption profiles for sight lines with increasing column density. The best-fit values for column density, rotational excitation temperature, and Doppler broadening parameter are listed. [See the electronic edition of the *Journal* for a color version of this figure.]

In these cases, the fit was limited to those lines with $W_\lambda/\lambda \sim (5-9) \times 10^{-6}$, depending on the data quality, to avoid saturation effects. The application of the equivalent width cut lowered the determined b -value and increased the determined N by, typically, 0.2 dex. The need for this approach was demonstrated best by our attempts to fit the HD 24534 (χ Per) sight line, the $N(\text{CO})$ of which was increased by 0.5 dex after the application of the equivalent width cut. Twelve bands of the $A-X$ system were clearly observed, but we could get no consistent fit from profile fitting. In addition, the COG shows deviations from what would be expected for a single set of fit parameters. This is most likely because of the presence of unresolved velocity components.

The CO absorption profiles for χ Per have been fit before using Goddard High-Resolution Spectrograph (GHRS) data of the $A-X$ system (Kaczmarczyk 2000) as well as STIS data of the inter-system bands (Sheffer et al. 2002). Kaczmarczyk (2000) found that a two-component model, with one component having 85% of the column, was necessary to get a good profile fit of the data. He derives a column of $N(\text{CO}) = (1.0 \pm 0.2) \times 10^{16} \text{ cm}^{-2}$, consistent with that found by Sheffer et al. ($1.41 \times 10^{16} \text{ cm}^{-2}$) as well as this study ($1.35 \times 10^{16} \text{ cm}^{-2}$). In principle, the unsaturated inter-system bands, as Sheffer et al. used, could also be used for the highest column density sight lines, but there were no STIS E140H

data available in the archive with the appropriate wavelength coverage for any of the other stars.

2.2. Molecular Hydrogen

H_2 has an extensive band system in the *FUSE* wavelength range ($912 \text{ \AA} \lesssim \lambda \lesssim 1110 \text{ \AA}$ at temperatures typical of the diffuse ISM) arising from electronic transitions out of the ground state ($X^1\Sigma_g^+$) to the Lyman ($B^1\Sigma_u^+$) and Werner ($C^1\Pi_u$) levels. These absorption lines were first used by *Copernicus* to characterize the average properties of the molecular phase of the ISM (Spitzer et al. 1974). More recently, *FUSE* has been used to compile large samples of H_2 absorption data for Galactic (Rachford et al. 2002; Gillmon et al. 2006) and extragalactic (Tumlinson et al. 2002) sight lines.

We have analyzed the H_2 absorption lines in the sight lines presented here with a least-squares fitting routine that compares the data to a model spectrum. The model spectrum was constructed with a power-law fit to the stellar continuum over the wavelength region of interest ($\approx 1035-1140 \text{ \AA}$) with absorption components derived using the H_2ools optical depth templates of McCandliss (2003). The continuum was placed interactively, as individual adjustments were necessary in almost all cases. The optical depth templates are calculated for each line using a Voigt profile, ensuring the correct line shape for different column density regimes.

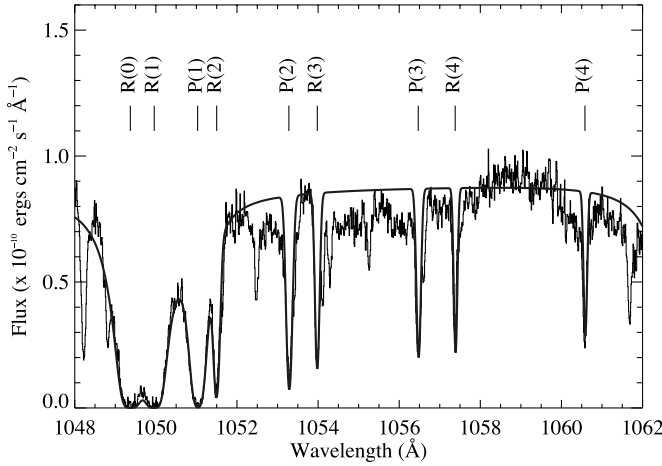


FIG. 2.— Sample H₂ absorption (HD 93205) of the Lyman (4–0) band system, with best-fit absorption profile overplotted. Absorptions out of the $J = 0–4$ are included in the fit; however, the $J = 0$ and 1 lines contain the majority of the column density, and only these are considered in determining the total H₂ column density. Other lines in the spectrum are from Ar I (1048.2 Å), Fe II (1055.3 Å), and high- J states of the Lyman (5–0) band. [See the electronic edition of the Journal for a color version of this figure.]

Figure 2 shows a sample absorption spectrum of H₂ and the best-fit model.

An iterative approach is used for absorption lines from rotational states from $J = 0$ to 4. A coarse grid of column densities [$15.6 < \log N(\text{H}_2(J)) < 23.0$] is scanned for b -values ranging from 2 to 11 km s⁻¹. This process establishes the column to within 0.25 dex and b -value to within ± 1 km s⁻¹. A fine grid of column

densities ($\Delta N = 0.01$ dex) is then scanned and the best fit is quoted to the nearest 0.05 dex. We feel that this is a conservative estimate of the accuracy of our H₂ column density determination. As a consistency check, we compare our results for two sight lines also studied by Rachford et al. (2002). The column densities measured for HD 185418 are identical to theirs within the errors. On the other hand, HD 102065 is discrepant in $\log N(0)$ by 0.2 dex.

This iterative approach proved repeatable for determining column densities for the $J = 0$ and 1 lines. The higher-lying rotational states ($J = 2–4$) were fit with the same procedure, initially scanning a grid of column densities from $10^{13}–10^{20}$ cm⁻². The quantitative results for these lines were less certain. Most of the lines arising from $J = 3$ and 4 fell on the “flat” part of the curve of growth (as well as those from $J = 2$ in a few cases) and were subject to the degeneracy between column density and b -value. In addition, some of the lines from $J = 2$ and 3 were blended, and we found that continuum placement was even more significant when dealing with these lines. To avoid these complications, we present only the columns derived for the $J = 0$ and 1 levels, as these states contain the majority of the molecular mass at diffuse ISM temperatures.

3. RESULTS

3.1. Column Densities and CO/H₂

Table 1 summarizes the derived column densities and rotational excitation temperatures for the CO and H₂ along the line of sight to each star, as well as the spectral type and reddening. For all but three of the sight lines in this study, we have obtained from the literature values for the neutral hydrogen

TABLE 1
MOLECULAR COLUMN DENSITIES AND ROTATIONAL TEMPERATURES

STAR	SPECTRAL TYPE	$E(B - V)$	CO			H ₂		CO/H ₂ ($\times 10^{-6}$)
			$\log N$ (cm ⁻²)	T_{rot} (K)	b (km s ⁻¹)	$\log N^a$ (cm ⁻²)	T_{rot} (K)	
HD 24534 ^b	B0 Ve	0.45	16.13 ± 0.20	5.3 ± 0.6	0.4 ± 0.2	20.92	57 ± 6	16.1 ± 8.3
HD 27778 ^b	B3 V	0.38	16.05 ± 0.14	6.1 ± 0.5	$0.7^{+0.3}_{-0.1}$	20.79	56 ± 6	18.0 ± 7.1
HD 91824	O7 V	0.27	≤ 13.60	19.99	61 ± 7	≤ 0.40
HD 93205	O3 V	0.37	13.23 ± 0.06	3.4 ± 0.6	4.3 ± 1.0	19.84	105 ± 21	0.24 ± 0.07
HD 93222	O7 III	0.40	13.36 ± 0.20	2.8 ± 1.0	0.7 ± 0.6	19.80	77 ± 11	0.36 ± 0.19
HD 93840	B1.0 Ib	0.14	13.38 ± 0.08	3.6 ± 0.6	$1.1^{+0.8}_{-0.5}$	19.55	47 ± 4	0.68 ± 0.21
HD 102065 ^c	B2V	0.31	13.62 ± 0.12	4.0 ± 1.0	1.7 ± 1.2	20.63	59 ± 7	0.10 ± 0.04
HD 103779	B0.5 III	0.21	≤ 12.35	19.90	86 ± 14	≤ 0.03
HD 104705	B0 Ib	0.26	12.98 ± 0.16	3.4 ± 0.8	$1.0^{+1.2}_{-0.5}$	19.98	92 ± 16	0.10 ± 0.04
HD 116852	O9 IV	0.22	13.28 ± 0.04	3.0 ± 0.3	$0.4^{+0.5}_{-0.1}$	19.85	70 ± 9	0.27 ± 0.07
HD 121968	B1 V	0.07	≤ 12.30	18.70	38 ± 3	≤ 0.40
HD 152723	O6.5 III	0.46	13.88 ± 0.15	4.0 ± 0.3	1.0 ± 0.2	20.33	73 ± 10	0.36 ± 0.15
HD 163758	O6.5 Iaf	0.35	13.42 ± 0.05	4.5 ± 0.5	1.3 ± 0.5	19.85	86 ± 14	0.37 ± 0.10
HD 177989	B0 III	0.25	14.62 ± 0.17	3.7 ± 0.4	0.7 ± 0.1	20.23	52 ± 5	2.4 ± 1.1
HD 185418	B0.5 V	0.50	14.82 ± 0.20	3.2 ± 1.1	$0.8^{+1.0}_{-0.3}$	20.79	105 ± 21	1.1 ± 0.6
HD 201345	O9 p	0.32	≤ 12.40	19.43	147 ± 41	≤ 0.09
HD 203532	B3 IV	0.32	15.70 ± 0.17	5.5 ± 0.3	0.7 ± 0.1	20.71	49 ± 5	9.8 ± 4.5
HD 206267 ^b	O6.5 V	0.52	16.11 ± 0.13	6.4 ± 0.5	$0.7^{+0.8}_{-0.1}$	20.86	64 ± 8	17.9 ± 6.8
HD 207198 ^b	O9.5 Ib	0.62	15.53 ± 0.20	3.7 ± 1.2	1.0 ± 0.5	20.83	66 ± 8	5.0 ± 2.6
HD 210839 ^b	O6 Infp	0.56	15.41 ± 0.08	4.4 ± 0.3	$0.9^{+0.2}_{-0.1}$	20.84	72 ± 10	3.7 ± 1.1
HD 218915	O9.5 Iab	0.29	13.64 ± 0.13	3.9 ± 0.2	1.6 ± 0.6	20.15	86 ± 14	0.31 ± 0.12
HD 303308	B1.0 III	0.30	13.65 ± 0.06	3.7 ± 0.4	3.1 ± 0.5	20.35	86 ± 14	0.20 ± 0.05
CPD -59 2603	O7 V	0.46	14.15 ± 0.10	3.2 ± 0.5	$0.6^{+0.3}_{-0.1}$	20.15	77 ± 11	1.00 ± 0.33

^a Errors are ± 0.10 .

^b H₂ values from Rachford et al. (2002).

^c Spectral Type and $E(B - V)$ determined this study.

TABLE 2
MOLECULAR AND ATOMIC HYDROGEN COLUMN DENSITIES

STAR	H ₂ COLUMN DENSITIES (cm ⁻²) ^a		H I		MOLECULAR FRACTION
	log <i>N</i> (0)	log <i>N</i> (1)	log <i>N</i> (cm ⁻²)	Ref.	
HD 24534 ^b	20.76	20.42	20.73	1	0.76
HD 27778 ^b	20.64	20.27	21.20	4	0.44
HD 91824.....	19.80	19.55	21.15	2	0.12
HD 93205.....	19.40	19.65	21.33	1	0.06
HD 93222.....	19.50	19.50	21.54	2	0.04
HD 93840.....	19.45	18.85	21.04	1	0.06
HD 102065.....	20.45	20.15	21.90	4	0.10
HD 103779.....	19.55	19.65	21.16	1	0.10
HD 104705.....	19.60	19.75	21.11	1	0.13
HD 116852.....	19.60	19.50	20.96	1	0.14
HD 121968.....	18.65	17.70	20.71	1	0.02
HD 152723.....	20.05	20.00	21.43	1	0.14
HD 163758.....	19.50	19.60	21.23	1	0.08
HD 177989.....	20.10	19.65	20.95	1	0.28
HD 185418.....	20.35	20.60	21.11	2	0.49
HD 201345.....	18.85	19.30	20.88	1	0.07
HD 203532.....	20.60	20.05	21.50	4	0.24
HD 206267 ^b	20.64	20.45	21.30	3	0.42
HD 207198 ^b	20.61	20.44	21.34	1	0.38
HD 210839 ^b	20.57	20.50	21.15	1	0.53
HD 218915.....	19.80	19.90	21.11	1	0.18
HD 303308.....	20.00	20.10	21.45	1	0.14
CPD -59 2603.....	19.85	19.85	21.46	1	0.09

^a Uncertainties for $N(0, 1) \approx \pm 0.1$.

^b H₂ values from Rachford et al. (2002).

REFERENCES.—(1) Diplas & Savage 1994; (2) Fitzpatrick & Massa 1990; (3) Rachford et al. 2002; (4) This study.

column density; the H I column densities for HD 27778, HD 102065, and HD 203532 were determined from Ly α fits to the STIS data. The spectral type for HD 102065 given in the literature of B9 IV is inconsistent with the presence of weak but notable C IV $\lambda\lambda 1548$ –1550 features typical of spectral types B1.5 V or slightly later for high-luminosity class (Walborn et al. 1995). Consequently, we adopt a B2 V spectral type for this object [$(B - V)_o = -0.24$], yielding $E(B - V) = 0.31$. Table 2 lists the column densities of the first two rotational states of H₂, the

column density of H I, and the molecular fraction $f = 2N(\text{H}_2)/[2N(\text{H}_2) + N(\text{H I})]$.

With both molecules there is a trend toward higher column density with increased reddening (see Fig. 3), although neither exhibits a tight correlation; for any given $E(B - V)$, the column density of both molecules can vary by at least an order of magnitude. The scatter is most likely a product of varying environments. The color excess is a measure of the total amount of dust along the line of sight, but may not necessarily reflect the geometrical distribution of the gas and dust; a single translucent cloud could produce the same reddening as a series of diffuse clouds (see, for example, the models of Kopp et al. 2000).

Figure 4 shows the correlation of CO with H₂. This is the tightest correlation seen in this study, roughly a power-law relationship, i.e., $N(\text{CO}) \propto N(\text{H}_2)^\alpha$, with $\alpha \approx 2$. At lower H₂ column densities, the CO can be difficult to observe, whereas along the higher column sight lines, CO increases very quickly. This is most likely an indication of the onset of CO self-shielding, but may also be attributed to increased shielding of CO from photo-dissociation by either H₂ or dust. Overplotted in Figure 4 are the results from the survey by Crenny & Federman (2004), which used *Copernicus* data and the Cep OB data from Pan et al. (2005), who used STIS and *FUSE* data in a manner similar to this work. Pan et al. note a systematic offset of the CO/H₂ relationship between the Cep OB2 and OB3 clusters, further indicating that differences in the physical conditions of the clouds are playing a strong role in the scatter in this relationship.

Contours show lines of constant CO/H₂. The slope of the correlation is steeper than 1, and thus, there is an increasing trend of the CO/H₂ with increasing column, with a steepening of the slope near a CO column of $\approx 10^{15}$ cm⁻², where the self-shielding of CO becomes important. The value of CO/H₂ reaches about 10^{-5} for the highest column sight lines, and if the general trend is extrapolated to a high H₂ column, it agrees well with the value for dense clouds of about 3×10^{-4} , as determined by Lacy et al. (1994) for NGC 2024 and NGC 2264. This trend is well supported theoretically, for example, by the models of van Dishoeck & Black (1988), which suggest that the column density ratio should increase from around 10^{-7} in diffuse clouds to 10^{-4} in dense clouds.

The left panel of Figure 5 shows CO/H₂ as a function of reddening. Again, the results of earlier studies are shown overplotted.

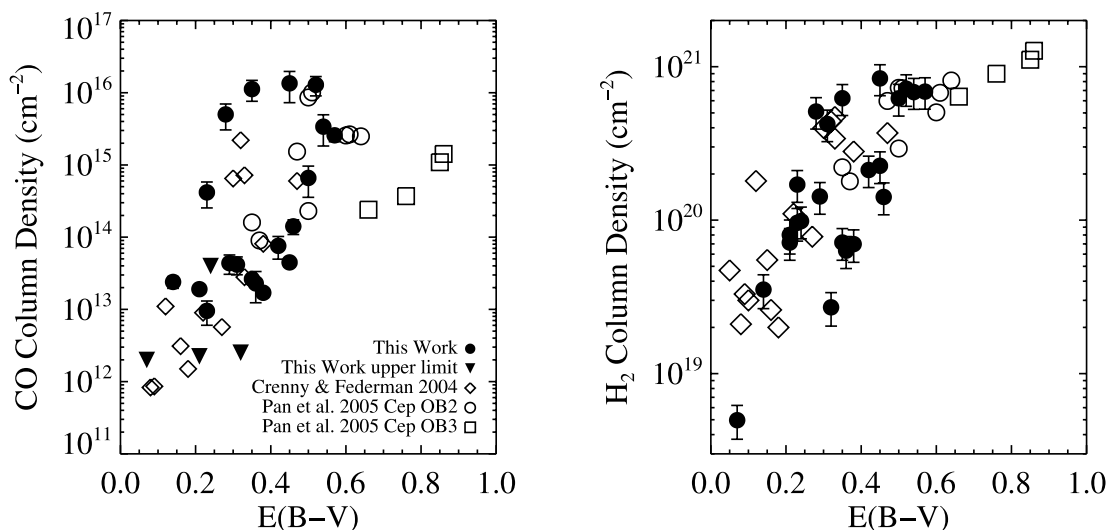


FIG. 3.—CO (left) and H₂ (right) column density vs. reddening, $E(B - V)$.

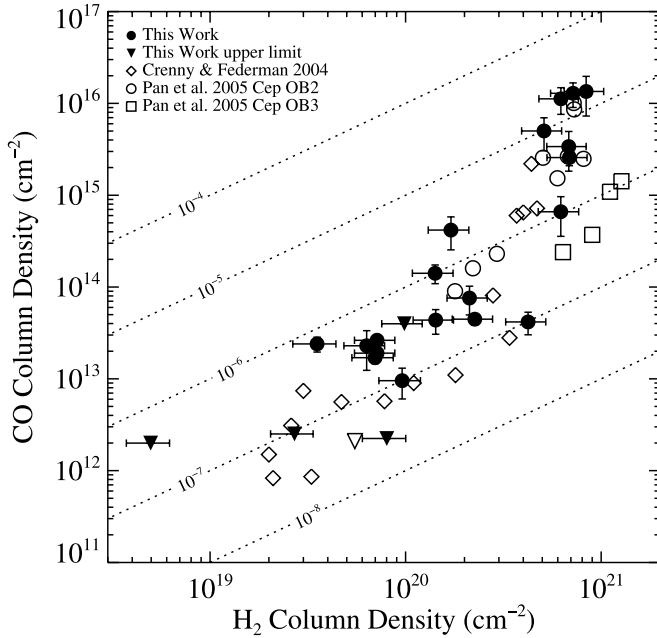


FIG. 4.— Correlation plot of CO with H₂ for the data presented in this study as well as previous studies. Contours of constant CO/H₂ are overlotted.

There is a general trend toward higher ratio with increased reddening. An interesting standout from this trend are the Cep OB3 data, which appear to have far smaller CO/H₂ for the $E(B - V)$ than expected.

The center panel of Figure 5 shows the ratio with respect to the molecular fraction. Below a molecular fraction of about 0.25 (the average value found in the Savage et al. [1977] study), the CO/H₂ is about 3×10^{-7} on average; we consider this the “diffuse” regime. These lines of sight have a significant spread in reddening, covering $0.07 \leq E(B - V) \leq 0.46$, and are not well differentiated from the high CO/H₂ sight lines in the plot versus reddening. The fact that they separate well from the high-ratio sight lines in this plot suggests that the molecular fraction represents a better measure of a cloud’s physical condition than $E(B - V)$. This is most likely because the amount of dust tends to follow the total hydrogen along the line of sight rather than the molecular component, and the destruction of these molecules is more sensitive to line-shielding than dust-shielding. Above a molecular fraction

of 0.25, there is marked increase in the ratio with increasing molecular fraction, with an average value of about 7×10^{-6} .

We see a similar behavior of the CO/H₂ with the traditional density measure A_V/d , where A_V is the magnitude of extinction in the V band and d is the distance to the star. Valencic et al. (2004) have compiled a large catalog of extinction properties to reddened Galactic O and B stars, and there is an overlap of 15 stars with this study. The right panel of Figure 5 shows CO/H₂ versus this density measure. Jenniskens & Greenberg (1993) found that $A_V/d = 0.9 \text{ mag kpc}^{-1}$ appears to separate the diffuse from the dense lines of sight, and our data show an increase in the CO/H₂ above $A_V/d \sim 1$; however, we would state that the division is between diffuse and translucent, as the sight lines in our study with $A_V/d > 1 \text{ mag kpc}^{-1}$ still have CO/H₂ about an order of magnitude less than that for dense clouds.

Further comparison to the Valencic et al. (2004) catalog produces no significant correlations of extinction curve parameters to the measured values of N or T_{rot} for either CO or H₂, or for CO/H₂. The study of Burgh et al. (2000) indicated a correlation between the CO column density normalized by $E(B - V)$ and the strength of the far-UV rise; however, that study, using data from the *International Ultraviolet Explorer* satellite, covered column densities ranging from $N(\text{CO}) = 10^{14}$ to 10^{18} cm^{-2} , the correlation only becoming apparent at the highest column densities and steepest UV curves. It is likely that in the environments of the clouds probed in this study, shielding by H₂ and self-shielding are more important in regulating the abundance of CO than dust-shielding, which may not play a significant role until $N(\text{CO}) > 10^{16}$.

3.2. Isotopic Fractionation

For six of the sight lines, absorption lines from the isotopic variant ¹³CO are observed. Table 3 lists the ¹²CO and ¹³CO column densities and rotational temperatures for these sight lines. The first column of ¹³CO column densities are those determined if it is assumed that the two isotopes have the same rotational temperature. Also listed are the results if the temperature is allowed to be a free parameter. The results give column densities within 0.2 dex of each other. Section 3.3 discusses the observed difference in rotational temperatures when that parameter is left free to be fit.

The isotopic ratio ¹²CO/¹³CO ranges from about 50 to 70, with an average value of 57 ± 7 , and we see no strong correlations

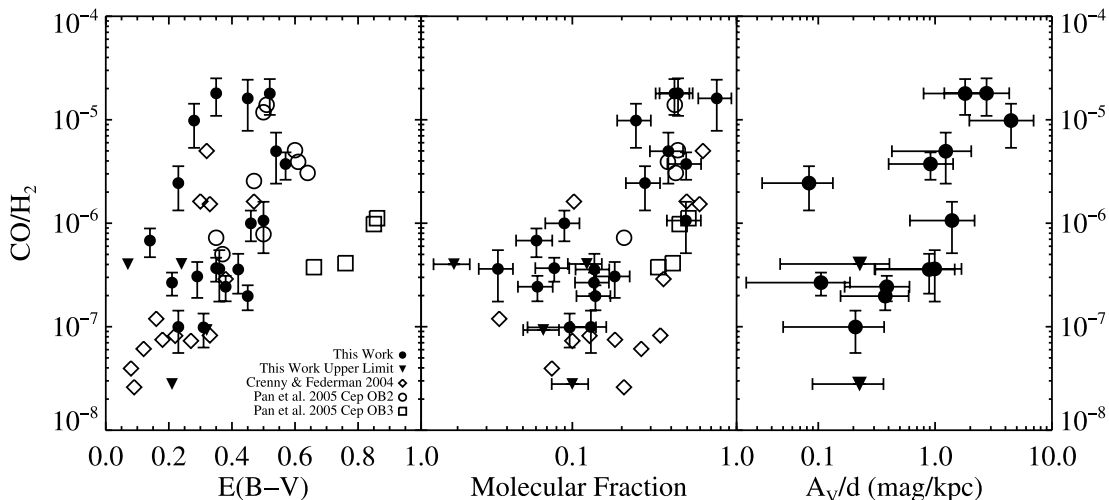


FIG. 5.— Left: CO/H₂ plotted vs. reddening. Center: CO/H₂ vs. molecular fraction. Right: CO/H₂ vs. average density (A_V/d).

TABLE 3
CO ISOTOPIC COLUMN DENSITIES AND ROTATIONAL TEMPERATURES

STAR	¹² CO		¹³ CO			¹² CO/ ¹³ CO	<i>T</i> ₁₂ / <i>T</i> ₁₃
	log <i>N</i> (cm ⁻²)	<i>T</i> _{rot} (K)	log <i>N</i> ^a (cm ⁻²)	log <i>N</i> (cm ⁻²)	<i>T</i> _{rot} (K)		
HD 24534	16.13 ± 0.20	5.3 ± 0.6	14.33	14.30 ± 0.12	4.1 ± 0.6	68 ± 31	1.3 ± 0.3
HD 27778	16.05 ± 0.13	6.1 ± 0.5	14.26	14.28 ± 0.08	3.9 ± 0.6	59 ± 14	1.6 ± 0.3
HD 177989	14.62 ± 0.17	3.7 ± 0.2	12.90	12.82 ± 0.08	3.9 ± 0.5	63 ± 25	1.0 ± 0.2
HD 203532	15.70 ± 0.17	5.5 ± 0.5	13.95	13.97 ± 0.20	4.8 ± 0.6	54 ± 21	1.1 ± 0.2
HD 206267	16.11 ± 0.17	6.4 ± 0.6	14.44	14.42 ± 0.08	6.4 ± 0.8	49 ± 15	1.0 ± 0.2
HD 210839	15.41 ± 0.04	4.5 ± 0.2	13.75	13.70 ± 0.10	3.5 ± 0.8	51 ± 9	1.3 ± 0.3

^a Column density assuming same *T*_{rot} as for ¹²CO.

with any other measurable quantity. The largest value is for χ Per (HD 24534), whose ratio was determined by Sheffer et al. (2002) to be 73 ± 12 , in good agreement with the value found here; however, we do not see the enhanced fractionation measured along such lines of sight as those to ρ Oph A, χ Oph (Federman et al. 2003), and ζ Oph (Lambert et al. 1994), with values of 125 ± 23 , 117 ± 35 , and ~ 170 , respectively.

Wilson & Rood (1994) review the literature for determinations of the interstellar ¹²C/¹³C and adopt a value of 77 ± 7 ; however, there is significant scatter among the values reported in the literature that seems to depend on the methods used, which can include millimeter emissions of C¹⁸O (e.g., Langer & Penzias [1993] who get ¹²C/¹³C = 57–74) and near-infrared spectroscopy of CO vibrational bands (e.g., Goto et al. [2003], who get ¹²C/¹³C = 86–137). One method that is not sensitive to processes of selective fractionation (described below) is determining the ¹²CH⁺/¹³CH⁺ ratio, and the recent measurements of Casassus et al. (2005) agree with a value of ~ 78 , but they interpret the scatter in their data (1 $\sigma = \pm 12.7$) as a true measure of chemical heterogeneity in the local ISM.

There are two main processes that can cause ¹²CO/¹³CO to deviate from the average ISM value of the ¹²C/¹³C isotope ratio. The first is isotopic charge exchange (Watson et al. 1976), which occurs in gas where C⁺ is in abundance, as might be expected in translucent clouds, and enhances the ¹³CO because of its lower zero-point energy. The other process is selective isotopic photodissociation (Bally & Langer 1982), which favors the more abundant, and thus more likely to self-shield, ¹²CO.

If isotopic exchange is more important than photodissociation, we would expect $^{12}\text{CO}/^{13}\text{CO} = \exp(-\Delta E/kT_{\text{kin}})(^{12}\text{C}/^{13}\text{C})$, where ΔE is the zero-point energy difference between the two isotopes ($\Delta E/k = 35$ K). The average kinetic temperature for these six sight lines is 58 K, and therefore, we could expect to see as low as half the average ISM isotopic ratio. However, it is unlikely that photodissociation does not play a role, and the models of van Dishoeck & Black (1988) suggest at best only a mild relative increase in the ¹³CO abundance for temperatures in the range seen in this sample.

3.3. Rotational Excitation

Both the *FUSE* and the STIS data are of high enough resolution to resolve the individual rotational transitions of H₂ and CO, respectively. This allows for the determination of the rotational excitation temperature. For both molecules the relative column densities in the *J* = 0 and 1 states are representative of the rotational excitation temperature of the gas, *T*₀₁, following

$$N(1)/N(0) = g_1/g_0 \exp(-E_{01}/kT_{01}),$$

where *N*(*J*) is the column density in the *J*th rotational state, *g*_{*J*} is the statistical weight, *E*₀₁ is the energy difference between the *J* = 0 and 1 states, and *k* is Boltzmann’s constant.

Transitions between the ground-state rotational states of H₂ are not dipole-allowed and have lifetimes long enough that at the densities typical of diffuse and translucent clouds, collisions dominate over other processes in determining the relative populations of the low-lying *J* levels. Thus, *T*₀₁ for H₂ traces the kinetic temperature of the gas. In CO, on the other hand, the rotational transitions are dipole-allowed and have short lifetimes such that the rotational excitation temperature will reflect mostly the density in the cloud, not the kinetic temperature.

The average H₂ temperature in our sample is 74 ± 24 K. This agrees very well with the value derived from *Copernicus* observations of 61 stars with H₂ columns greater than 10^{18} cm⁻² of $\langle T_{01} \rangle = 77 \pm 17$ K (Savage et al. 1977) as well as the $\langle T_{01} \rangle = 68 \pm 15$ K of Rachford et al. (2002). The higher *J* levels can be populated through collisions, UV- and formation-pumping, and radiative cascade, and thus their relative populations may not reflect the kinetic temperature. The absorptions from these levels is not considered in this study and should not greatly affect the column density determinations, because the *J* = 0 and 1 absorption accounts for the vast majority of the H₂ column.

There is no correlation of the rotational temperatures of either H₂ or CO with reddening along the line of sight, nor was any seen in either the *Copernicus* study or the *FUSE* study of Rachford et al. (2002). The rotational temperatures are also independent of total H₂ column density. However, there are several interesting relationships with rotational temperature.

Rachford et al. (2002) point out that for lines of sight dominated by translucent clouds, the molecular fraction should be large, while the kinetic temperature is small. Although we do not see a strong correlation (i.e., we see several sight lines with low temperature and molecular fraction), all of the sight lines with above average H₂ temperature have a molecular fraction below 0.2, except for HD 185418, which has a molecular fraction of 0.49.

For CO column densities less than 10^{15} cm⁻², the average rotational excitation temperature is 3.6 ± 0.5 K. For the higher column density sight lines, the average is 5.2 ± 1.0 K. In addition, the average CO rotational temperature is 4.5 ± 1.1 K for sight lines with below average H₂ temperature, and 3.5 ± 0.5 K for those above (see Fig. 6). The increase of excitation with column density may be a result of “photon trapping” in clouds of higher optical depth. As the optical depth of the 2.6 mm *J* = 1–0 radio line increases, it becomes more likely that the photon will be re-absorbed by another CO molecule. This hinders the radiative cooling, and the collisional excitation/de-excitation process with the surrounding H₂ molecules will equilibrate at a higher rotational

temperature. The CO T_{rot} is thus sensitive to the H₂ space density, the H₂ kinetic temperature, and the line center optical depth, which itself depends on the column density and b -value.

Using an online statistical equilibrium radiative transfer code,² (Schöier et al. 2005), we determined that the increase in temperature for the higher column density sight lines is consistent with the photon trapping effect in clouds with H₂ space densities in the 20–100 cm⁻³ range, assuming our average H₂ temperature as the kinetic temperature and a b -value of about 0.6 km s⁻¹. This code assumes a single, homogeneous cloud, which may not necessarily represent a sight line with multiple velocity components.

Another method for increasing the rotational excitation of CO is that of radiative pumping from nearby dense clouds, as studied by Wannier et al. (1997). This effect will be proportional to the solid angle subtended by the nearby cloud as viewed from the CO along the line of sight when the relative velocity between the absorbing and emitting clouds is zero. They point out that for sight lines with space densities of a few hundred per cubic centimeter and with kinetic temperatures in the range of the H₂ temperatures, we observe that fractions of ~ 0.2 of 4π steradians are enough to account for the increased CO temperatures observed.

Wannier et al. (1997) point out that this effect may be differentiated from collisional excitation by observing other isotopes of CO, because the lower brightness temperature of the nearby clouds will reduce the rate of radiative pumping. Table 3 lists the ¹³CO temperatures derived in this study, with the isotopic temperature ratio T_{12}/T_{13} listed in the final column. For two or possibly three of the sight lines, there is an increased relative temperature for the more abundant isotope. These are also the sight lines with the higher molecular fractions, and are perhaps sight lines that pass through the outer portions of a denser molecular cloud, where a larger fraction of its sky may be covered by optically thick, radiating gas. However, we note that the photon trapping could also explain the T_{12}/T_{13} , because the less optically thick ¹³CO would not have its rotational temperature enhanced by the effect.

4. DISCUSSION

The traditional view of the ISM differentiates between diffuse and translucent clouds, where the transition occurs at about $A_V = 1$. However, recent studies (Rachford et al. 2002; Sonnentrucker et al. 2003) have suggested that there is not a clear distinction and argue that perhaps none of the sight lines they see have truly “translucent” clouds, which models expect to show molecular fractions reaching nearly 1. This situation could arise from having multiple “diffuse” clouds along the line of sight, adding up to a given A_V . This would result in $E(B - V)$ not necessarily being a good measure of the physical properties along a given line of sight, and our study confirms this.

It is thus more important to measure parameters that are better representative of the physical state of the clouds. The molecular fraction gives one such measure but, for reasons laid out in Rachford et al. (2002), may not allow for the unambiguous separation of diffuse and translucent sight lines. However, the CO molecule is more sensitive to photodissociative processes and can be used to probe the transition region between diffuse and translucent clouds. Kopp et al. (2000) model the sensitivity of the abundance of CO to the effects of geometry, dust shielding, and fragmentation of the ISM. Their results suggest that if a sight line were simply a collection of small, diffuse clouds, then we would not expect to see an increased CO/H₂ with total column density.

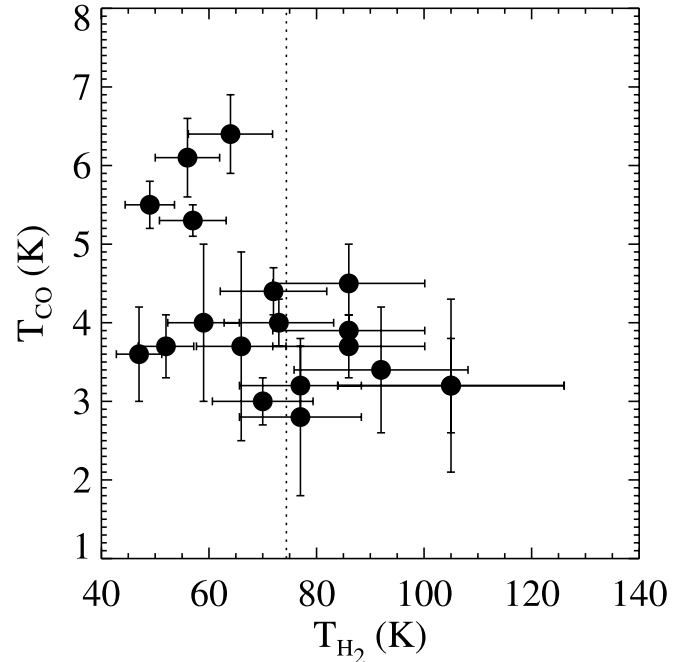


FIG. 6.—CO rotational excitation temperature vs. H₂ rotational excitation temperature. The vertical dotted line is at the average value for the H₂ temperature. Only sight lines with below-average H₂ temperature exhibit enhanced CO temperature.

The increase in CO/H₂ that we observe with increased molecular fraction suggests that these sight lines do begin to sample the translucent regime.

We believe that the transition from low to high CO/H₂ is similar to the one that hydrogen undergoes when the H₂ column density gets high enough for self-shielding to take effect. The molecular fraction observed in a cloud will be dependent on the balance of the formation and the photodestruction. Savage et al. (1977) found that the molecular fraction transitions from “low” (< 0.01) to “high” (> 0.01) values at about $N_{\text{H}} = 5 \times 10^{20}$ cm⁻², which corresponds to $E(B - V) \sim 0.08$. This is also seen for high-latitude Galactic sight lines (Gillmon et al. 2006). The location of this transition is dependent on the physical conditions in the ISM, including the H₂ formation rate on grains, the intensity of the interstellar radiation field, and the degree of fragmentation of molecular clouds along the line of sight. The behavior of the Galactic sight lines is in marked contrast to that of the Magellanic Clouds (Tumlinson et al. 2002), in which this transition occurs at much larger columns, perhaps because of the lower H₂ formation rates and higher dissociating radiation fields. All of the sight lines in this study have total hydrogen columns above this transition value, and should be considered part of the “high” molecular fraction regime.

The values of CO/H₂ that we measure for the diffuse and translucent regimes range from 10^{-7} to 10^{-5} , in contrast with the canonical dense cloud value of 10^{-4} . This discrepancy is consistent with the studies of de Vries et al. (1987) and Magnani et al. (1998), which find variations in the X -factor as determined from radio observations of high-latitude translucent clouds. Both studies interpret their results as variations of the CO abundance, which could have a deleterious effect on the process of determining the masses of individual clouds. It could also impact the “weighing” of galaxies if the diffuse or translucent ISM contribute significantly to the CO radio emission. Polk et al. (1988) found, based on the ratios of integrated ¹²CO and ¹³CO emission, that a significant

² Available at <http://www.strw.leidenuniv.nl/~moldata>.

contribution to the total ^{12}CO emission from a galaxy could be arising from material of moderate optical depth. In that case, applying a standard X -factor, derived from the dense clouds, would result in the underestimation of the total mass because of the lower CO/H_2 in the more diffuse gas.

This difference could be particularly important for clouds subjected to intense UV radiation fields. Yao et al. (2003) found in their study of CO emission in starburst galaxies an X -factor significantly lower than the standard Galactic value. Furthermore, they found, by virial analysis, that the clouds in these galaxies were not gravitationally bound unless the CO/H_2 was 9–90 times lower than expected and suggest that the CO emission arises from nonvirialized warm and diffuse gas clouds. On the other hand, Rosolowsky et al. (2003) find no evidence in M33 for a diffuse molecular component traced by CO emission, concluding that most of the CO flux resides in the giant molecular clouds.

The direct comparison of the column densities determined from UV absorption line spectroscopy of CO and H_2 provides a technique for probing the structure and chemical balance of the ISM free from many of the biases and assumptions inherent in the traditional X -factor method. If the CO $J = 1-0$ radio emission along these lines of sight could be measured, then the relationship between CO/H_2 and the X -factor could be checked directly. It would also be useful to use absorption spectroscopy to explore the sight lines with $N(\text{H}_2) = 10^{21}-10^{22} \text{ cm}^{-2}$, the regime in which we expect to see the transition from translucent to dense clouds. The power-law increase in CO versus H_2 seen in the diffuse/translucent regime should turn over as A_V rises above ~ 3 and the CO/H_2 “saturates” at the canonical dense cloud value of $\sim 10^{-4}$.

Furthermore, extragalactic environments could be explored, such as the Magellanic Clouds; however, we do expect that with the currently available archival data, CO will be difficult to detect there. The study of Tumlinson et al. (2002) found that although H_2 column densities as high as around 10^{20} cm^{-2} have been detected, the typical columns found in the Clouds lie in the $10^{15}-10^{19} \text{ cm}^{-2}$ range. If the CO/H_2 ratio were to follow the trend seen in the Galactic sample, the CO column densities would be below the STIS detection threshold. We would expect, however, that the CO/H_2 would be even lower because of the lower metallicity and higher UV radiation fields seen in the Clouds. Yet, because models predict (e.g., Bell et al. 2006) the CO/H_2 to change with environment, if the appropriate data were taken, the technique could be used to explore the varying conditions in the diffuse/translucent ISM in other galaxies as well as our own.

The authors would like to thank Chris Howk for helping with the initial archive search and B-G Andersson for valuable input. E. B. B. would like to thank Jay Gallagher and John Mathis for useful discussions. The authors would also like to thank the referee for very useful suggestions, particularly those that led to a more robust fitting method used in fitting high column density sight lines with unresolved velocity structure. All of the data presented in this paper were obtained from the Multimission Archive at the Space Telescope Science Institute (MAST). STScI is operated by the Association of Universities for Research in Astronomy, Inc., under NASA contract NAS 05-26555. Support for MAST for non-*HST* data is provided by the NASA Office of Space Science via grant NAG 05-7584 and by other grants and contracts.

REFERENCES

- Bally, J., & Langer, W. D. 1982, *ApJ*, 255, 143
 Bell, T. A., Roueff, E., Viti, S., & Williams, D. A. 2006, *MNRAS*, 371, 1865
 Burgh, E. B., McCandliss, S. R., Andersson, B-G, & Feldman, P. D. 2000, *ApJ*, 541, 250
 Casassus, S., Stahl, O., & Wilson, T. L. 2005, *A&A*, 441, 181
 Crenny, T., & Federman, S. R. 2004, *ApJ*, 605, 278
 de Vries, H. W., Thaddeus, P., & Heithausen, A. 1987, *ApJ*, 319, 723
 Dickman, R. L. 1978, *ApJS*, 37, 407
 Diplas, A., & Savage, B. D. 1994, *ApJS*, 93, 211
 Federman, S. R., Glassgold, A. E., Jenkins, E. B., & Shaya, E. J. 1980, *ApJ*, 242, 545
 Federman, S. R., Lambert, D. L., Sheffer, Y., Cardelli, J. A., Andersson, B-G, van Dishoeck, E. F., & Zsargó, J. 2003, *ApJ*, 591, 986
 Fitzpatrick, E. L., & Massa, D. 1990, *ApJS*, 72, 163
 Gillmon, K., Shull, J. M., Tumlinson, J., & Danforth, C. 2006, *ApJ*, 636, 891
 Goto, M., et al. 2003, *ApJ*, 598, 1038
 Jenniskens, P., & Greenberg, J. M. 1993, *A&A*, 274, 439
 Kaczmarczyk, G. 2000, *MNRAS*, 316, 875
 Kopp, M., Roueff, E., & Pineau des Forêts, G. 2000, *MNRAS*, 315, 37
 Lacy, J. H., Knacke, R., Geballe, T. R., & Tokunaga, A. T. 1994, *ApJ*, 428, L69
 Lambert, D. L., Sheffer, Y., Gilliland, R. L., & Federman, S. R. 1994, *ApJ*, 420, 756
 Langer, W. D., & Penzias, A. A. 1993, *ApJ*, 408, 539
 Magnani, L., Onello, J. S., Adams, N. G., Hartmann, D., & Thaddeus, P. 1998, *ApJ*, 504, 290
 McCandliss, S. R. 2003, *PASP*, 115, 651
 Morton, D. C., & Noreau, L. 1994, *ApJS*, 95, 301
 Pan, K., Federman, S. R., Cunha, K., Smith, V. V., & Welty, D. E. 2004, *ApJS*, 151, 313
 Pan, K., Federman, S. R., Sheffer, Y., & Andersson, B-G 2005, *ApJ*, 633, 986
 Polk, K. S., Knapp, G. R., Stark, A. A., & Wilson, R. W. 1988, *ApJ*, 332, 432
 Rachford, B. L., et al. 2002, *ApJ*, 577, 221
 Rosolowsky, E., Engargiola, G., Plambeck, R., & Blitz, L. 2003, *ApJ*, 599, 258
 Savage, B. D., Bohlin, R. C., Drake, J. F., & Budich, W. 1977, *ApJ*, 216, 291
 Schöier, F. L., van der Tak, F. F. S., van Dishoeck, E. F., & Black, J. H. 2005, *A&A*, 432, 369
 Sheffer, Y., Federman, S. R., & Lambert, D. L. 2002, *ApJ*, 572, L95
 Shull, J. M., & Beckwith, S. 1982, *ARA&A*, 20, 163
 Spitzer, L., Cochran, W. D., & Hirshfeld, A. 1974, *ApJS*, 28, 373
 Sonnentrucker, P., Friedman, S. D., Welty, D. E., York, D. G., & Snow, T. P. 2003, *ApJ*, 596, 350
 Strong, A. W., & Mattox, J. R. 1996, *A&A*, 308, L21
 Tumlinson, J., et al. 2002, *ApJ*, 566, 857
 Valencic, L. A., Clayton, G. C., & Gordon, K. D. 2004, *ApJ*, 616, 912
 van Dishoeck, E. F., & Black, J. H. 1988, *ApJ*, 334, 771
 Walborn, N. R., Parker, J. W., & Nichols, J. S. 1995, *IUE Atlas of B-Type Spectra from 1200 to 1900 Å* (NASA RP-1363; Washington: NASA)
 Wannier, P., Penprase, B. E., & Andersson, B-G 1997, *ApJ*, 487, L165
 Watson, W. D., Anicich, V. G., & Huntress, W. T. 1976, *ApJ*, 205, L165
 Wilson, T. L., & Rood, R. 1994, *ARA&A*, 32, 191
 Yao, L., Seaquist, E. R., Kuno, N., & Dunne, L. 2003, *ApJ*, 588, 771
 Young, J. S., & Scoville, N. Z. 1991, *ARA&A*, 29, 581